Title

Severe SAR-CoV-2 infection in humans is defined by a shift in the serum lipidome resulting in dysregulation of eicosanoid immune mediators

Benjamin Schwarz[1&], Lokesh Sharma[2&], Lydia Roberts[1&], Xiaohua Peng[2], Santos Bermejo[2], Ian Leighton[1], Arnau Casanovas Massana[3], Shelli Farhadian[4], Albert I. Ko[3], Yale IMPACT Team, Charles S. Dela Cruz[2$*], Catharine M. Bosio[1$*]

[1]Laboratory of Bacteriology, National Institute of Allergy and Infectious Diseases, National Institutes of Health, Hamilton, MT, USA [2]Section of Pulmonary and Critical Care and Sleep Medicine, Yale University School of Medicine, New Haven, Connecticut [3]Department of Epidemiology of Microbial Diseases, Yale School of Public Health, New Haven, CT 06520 [4]Department of Medicine, Section of Infectious Diseases, Yale University School of Medicine, New Haven, CT, 06520

[&]Authors contributed equally

[$]Authors contributed equally

***Corresponding authors:**

Catharine M Bosio: bosioc@niaid.nih.gov

Charles S. Dela Cruz: Charles.delacruz@yale.edu

Abbreviations

LM-eicosanoid and docosanoid lipid mediators, PE-phosphatidylethanolamine, LPE- lyso-PE, PC-phosphatidylcholine, LPC-lyso-PC, PS-phosphatidylserine, PE(O) or PE(P)- plasmenyl or plasmanyl plasmalogen, TAG- triacylglycerol, DAG-diacylglycerol, MAG-monoacylglycerol, CE-cholesterol ester, Cer-

ceramide, DCer- dihydroceramide, HCer-hexosylceramide, LCer-lactosylceramide, SM-sphingomyelin, FAC-frees fatty acid, Rv-resolvin, LX-lipoxin, LT-luekotriene, HETE- hydroxyeicosatetraenoic acid, HEPE- hydroxyeicosapentaenoic acid, HDHA- hydroxydocosahexaenoic acid, HDPA- hydroxydocosapentaenoic acid, PG-prostaglandin, PD- D-series protectin, TxB2- Thromboxane B2, LC-MS/MS- liquid chromatography tandem mass spectrometry, CBA- cytometric bead array, PCA- principle component analysis, PLSDA- partial least square discriminant analysis

Introductory Paragraph

The COVID-19 pandemic has affected more than 10 million people worldwide with mortality exceeding half a million patients. Risk factors associated with severe disease and mortality include advanced age, hypertension, diabetes, and obesity.[1] Clear mechanistic understanding of how these comorbidities converge to enable severe infection is lacking. Notably each of these risk factors pathologically disrupts the lipidome and this disruption may be a unifying feature of severe COVID-19.[1-7] Here we provide the first in depth interrogation of lipidomic changes, including structural-lipids as well as the eicosanoids and docosanoids lipid mediators (LMs), that mark COVID-19 disease severity. Our data reveal that progression from moderate to severe disease is marked by a loss of specific immune regulatory LMs and increased pro-inflammatory species. Given the important immune regulatory role of LMs, these data provide mechanistic insight into the immune balance in COVID-19 and potential targets for therapy with currently approved pharmaceuticals.[8]

14 **Main Text**

15 Lipids function in disease to rearrange cellular signaling structures, modify metabolic processes, absorb
16 reactive species, and act directly as both autocrine and endocrine ligands in the regulation of the
17 immune system. Susceptibility to COVID-19 disease is strongly associated with pre-existing conditions
18 characterized by dysregulation of the lipidome and metabolome.[4-6] While several studies have examined
19 the systemic metabolic correlates of COVID-19, a well resolved interrogation of the lipidomic changes in
20 COVID-19 severity has not been pursued.[9-12] To measure lipidomic changes in COVID-19 and gain
21 mechanistic insights into how these changes may drive disease severity, we used serum draws from 19
22 healthy patients (healthy), 18 COVID-19 patients who did not require ICU admission (moderate) and 20
23 patients that required ICU admission (severe). The demographics, preexisting conditions, and treatment
24 details of these patients are indicated in Table 1. Lipid and metabolite measurements were made using
25 a series of targeted LC-MS/MS methods providing high-confidence feature identification.[13,14]
26 Importantly for lipidomic analysis, this enabled the resolution of acyl-chain length and degree of
27 unsaturation, which are both essential for understanding structural and functional rearrangement of the
28 lipidome.

29 Changes in primarily polar metabolites among COVID-19 patient cohorts from China, Italy, and France
30 have been reported.[9-12] In agreement with those studies, we observed a dysregulation of amino acid
31 pools, interruption of the glucose to lactate balance, and dysregulation of nucleotide catabolic products
32 such as xanthine, hypoxanthine, and urate (Sup. Fig. 1a-d).[9-12] These indicators suggest a robust
33 xanthine oxidase stress response, associated with heart disease,[15-17] and likely reflect the degree of
34 hypoxia/hypoxemia in the patient, which is a known to be associated with COVID-19 mortality.[18-22] These
35 data also indicate broad agreement across international populations in metabolic correlates of COVID-
36 19.

37 We next measured lipidomic profiles across severe and moderate COVID-19 infection along with the
38 healthy controls. To ensure comprehensive recovery of lipid classes, we utilized a modified chloroform
39 extraction method to recover both neutral and polar lipids.[23-25] By unbiased principle component
40 analysis (PCA), infected patients segregated from healthy in the negative ionization dataset but
41 overlapped in the positive ionization dataset (Sup. Fig. 2a-d). Group-biased partial least square
42 discriminant analysis (PLSDA) of the combined lipid dataset shows non-overlapping healthy and infected
43 separation across the primary axis of variance and a subgroup of severe patients that separate across
44 the secondary axis of variance (Fig. 1a). Specifically, the infected cohorts were associated with increased
45 levels of free poly-unsaturated fatty acids (PUFAs), rearrangement of certain sphingomyelins, and
46 decreased levels of PUFA-containing plasmalogens (Fig. 1b). Parallel univariate analysis revealed that
47 numerous neutral lipids significantly varied between severe and healthy controls, which may reflect
48 either changes in metabolism during infection or pre-infection differences in lipid levels due to pre-
49 existing conditions such as obesity (Sup. Fig 2e-g). Minor patterns distinguishing both infected from
50 healthy cohorts and moderate from severe disease were observed across lysophospholipids (Sup. Fig.
51 2h-j), cholesterol esters (chol-est) (Sup. Fig. 2k-m), and sphingolipids (Sup. Fig. 2n-p).
52 Across all lipid classes, PUFA containing lipids were abundant amongst the pool significantly varied lipids
53 between COVID-19 patients and healthy controls (Fig. 1c-e). To examine the regulation of PUFAs
54 between lipid classes and patient groups, we categorized lipids containing C20:4, C20:5, C22:5 or C22:6,
55 which likely represent arachidonic acid (AA), eicosapentaenoic acid (EPA), docosapentaenoic acid (DPA),
56 and docosahexaenoic acid (DHA). Of these PUFA-containing families, changes in the C20:4 series were
57 overrepresented in infected cohorts and could distinguish the severe from the moderate disease
58 patients (Fig. 1c-e). Many of these differentially regulated C20:4 species were the same plasmalogen
59 species that drove separation between infected and healthy cohorts by PCA (Sup. Fig. 2b) and PLSDA
60 (Fig. 2b, f-h). Interestingly, the depletion of PUFA-containing plasmalogen and increased levels of the

61 corresponding free-fatty acids (FAC) indicates the disease progression from the moderate to the severe
62 disease across each PUFA family (Fig. 1i-l). Plasmalogen is known to be a primary pool of PUFAs in both
63 immune and structural cells.[2,26] Upon systemic immune activation, PUFAs are liberated from their parent
64 glycerolipids and subsequently converted to a wide variety of immune signaling eicosanoids and
65 docosanoids.[27-32] The balance between pro-inflammatory, immune-regulating, and pro-resolving lipid
66 mediators can drastically change the efficacy of the immune response during infectious and sterile
67 inflammatory diseases as well as during the successful resolution of inflammation following disease.[33-35]
68 Therefore, we assessed the correlation of the eicosanoid and docosanoid species with COVID-19 disease
69 severity. We targeted 67 eicosanoid and docosanoid species using LC-MS/MS and 15 cytokines by
70 Cytometric Bead Array (CBA) or ELISA to relate lipid changes to markers of disease severity. Eicosanoid
71 and docosanoid lipid mediator (LM) signals were assessed by comparison to standards and available
72 spectral libraries (Sup. Fig. 3-5).[36] PCA analysis of the combined LM and cytokine data showed separation
73 of infected and healthy cohorts and overlapping, but distinct, separation between moderate and severe
74 patients (Fig. 2a). Nearly all LMs measured were positively correlated with infection (Fig. 2b). Univariate
75 analysis showed significant enrichment of the majority of LMs measured in both the moderate and
76 severe groups (Fig. 2c, d). Interestingly, moderate and severe disease were characterized by unique
77 milieus of LMs and cytokines (Fig. 2b, e). Moderate disease was characterized by significantly higher
78 levels of the pro-resolving LM resolvin E3 (RvE3). Further, there was a trend toward increased presence
79 of the prostaglandin family members, particularly PGE2 (p= 0.105), PGFD2 (p= 0.220) and PGF2a (p=
80 0.242). In contrast, severe disease was characterized by a further increase in free PUFAs levels, AA-, EPA-
81 , DPA and DHA-derived mono-hydroxylated species and AA-derived dihydroxylated species (Fig. 2c-e).
82 This shift in specific immune regulatory LMs in severe disease suggests that an imbalance of LMs may
83 contribute to disease progression. LMs are generated by a single or a series of oxygenase mediated
84 conversions of the parent PUFA. To examine the potential contribution of each oxygenase enzyme to

85 the severe disease phenotype we grouped LMs according to synthesis pathway (Fig. 2g-k). Several LMs
86 are shared between multiple enzyme groups as they require sequential stereospecific hydroxylations.
87 This grouping revealed that moderate disease was characterized by higher cyclooxygenase activity (COX)
88 as well as certain products of ALOX12 while severe disease is characterized by greater activity of ALOX5
89 and cytochrome p450 (CYP) enzymes. This is good agreement with previous observations from
90 influenza, which associated symptom severity with ALOX5 activity.[37]
91 COVID-19 comorbidities including obesity, age, heart disease, and diabetes are characterized by
92 dysregulation of the homeostatic lipidome.[1,3] To assess the correlation of these conditions with the
93 shifts in LM pools and their glycerolipid precursors, we overlaid age, sex, BMI, diabetes, heart disease,
94 survival, and antiviral treatment onto the separate PCAs (Sup. Fig. 7-15). Age and sex were evenly
95 distributed across the infected cohort on all PCAs (Sup. Fig. 7, 8). Of the treatments examined, only
96 remdesivir showed a negative correlation with the disease severity (Sup. Fig. 9-11). BMI, diabetes, heart
97 disease and morbidity segregated with the severity of disease across all datasets (Sup. Fig. 12-15). From
98 this study, it is likely that the lipidomic imbalance associated with severe disease is at least partially a
99 consequence of homeostatic disruption of the lipidome due to these pre-existing conditions. It is likely
100 that these pre-existing lipidomic imbalances are further exacerbated during COVID-19 through
101 dysregulation of the LM response resulting in severe disease, impaired resolution and persistent
102 inflammation.
103 Elevation of ALOX5- and CYP-dependent LMs in severe COVID-19 patient sera suggested systemic
104 upregulation of these pathways. To examine the cellular origin of these enzymes in COVID-19 patients,
105 we interrogated a published single cell RNAseq dataset of COVID-19 patient PBMCs for expression of
106 ALOX and CYP genes (Sup. Fig. 6a, b).[38] *ALOX5* expression was detected in most of the 20 cell types
107 identified (Fig. 3a-b) with the highest expression in CD14 monocytes, CD16 monocytes, neutrophils, B
108 cells, and DCs (Fig. 3c). *ALOX5* expression was significantly increased in neutrophils and trended upward

109 in CD14 monocytes, CD16 monocytes, and developing neutrophils (a population found almost
110 exclusively in diseased individuals) from COVID-19 patients compared to healthy controls. Interestingly,
111 severe COVID-19 is characterized by elevated *ALOX5* expressing monocyte/macrophage population and
112 depletion of lymphocyte populations.[38-40] The absence of CYP genes in the blood was consistent with
113 the primarily hepatic localization of these enzymes.[41] These data suggest a systemic dysregulation of
114 ALOX5 and further support the metabolic dysregulation of the liver in severe disease.[42]
115

116 **Conclusion**

117 These results provide the first detailed lipidomic understanding of COVID-19 disease progression and
118 represent one of the first combinations of bulk lipidomic and eicosanoid data to map mobilization of
119 lipids in human infectious disease.[7,37] We provide evidence that a systemic lipid network consisting of
120 liberated PUFAs from plasmalogen and their subsequent conversion to LMs, capable of modulating
121 inflammatory responses, characterizes both the onset and severity of COVID-19. Specifically, the loss of
122 the immune regulatory prostaglandins and the increased production of AA-derived products of ALOX5
123 and cytochrome P450 provides both a measure of disease severity and a mechanistic understanding of
124 the immune balance allowing for patient recovery. [43] Importantly, these pathways are directly
125 targetable with drugs previously approved for use in other inflammatory conditions and, thus, provide
126 therapeutic opportunities to control severe COVID-19.[27,31]

127

Acknowledgements

We are deeply indebted to the patients and families of patients for their contribution to this study. Prof. Charles N. Serhan and his group including, K. Boyle, A. Shay, C. Jouvene, X. de la Rosa, S. Libreros, and N. Chiang generously provided methodology, consultation and extensive training for the assessment of lipid mediators by LC-MS/MS. AB Sciex in particular M. Pearson, P. Norris and P. Baker (currently Avanti Polar Lipids) provided LC-MS/MS consultation and methods. Lokesh Sharma is supported by Parker B Francis Fellowship. Charles Dela Cruz is supported by Veterans affairs Merit Grant (BX004661) and Department of Defense grant (PR181442). Albert Ko and Charles Dela Cruz are supported by a U19 supplement for this work (AI089992-09S2). This work was supported by the Intramural Research Program of the National Institutes of Health, National Institute of Allergy and Infectious Diseases. This work was supported by the Department of Internal Medicine at the Yale School of Medicine, Yale School of Public Health, and the Beatrice Kleinberg Neuwirth Fund.

Author Contributions

B.S., L.S., C.D.C and C.M.B. conceived of experiment. L.S., X.P., S.B., A.C.M, S. F. and A.I.K and the Yale IMPACT Team enrolled patients and collected samples. B.S., L.R. and I.L. extracted samples and collected data. B.S. conducted metabolomics and lipidomics analysis. L.R. conducted single cell RNAseq analysis and cytokine analysis. B.S., L.R., L.S., C.D.C. and C.M.B wrote the manuscript. Yale Impact team: (Listed in alphabetical order) Kelly Anastasio, Michael H. Askenase, Maria Batsu, , Sean Bickerton, Kristina Brower, Molly L. Bucklin, Staci Cahill, , Yiyun Cao, Edward Courchaine, , Giuseppe DeIuliis, John Fournier, Bertie Geng, Laura Glick, Akiko Iwasaki, Nathan Grubaugh, Chaney Kalinich, William Khoury-Hanold, Daniel Kim, Lynda Knaggs, Maxine Kuang, Eriko Kudo, Joseph Lim, Melissa Linehan, Alice Lu-Culligan, , Anjelica Martin, Irene Matos, David McDonald, Maksym Minasyan, M. Catherine Muenker, Nida Naushad, Allison Nelson, Jessica Nouws, , Abeer Obaid, Camilla Odio, Saad Omer, Isabel Ott, Annsea Park, Hong-Jai Park,

Mary Petrone, Sarah Prophet, Harold Rahming, Tyler Rice, Kadi-Ann Rose, Lorenzo Sewanan, Denise Shepard, Erin Silva, Michael Simonov, Mikhail Smolgovsky, , Nicole Sonnert, Yvette Strong, Codruta Todeasa, Jordan Valdez, Sofia Velazquez, Pavithra Vijayakumar, Annie Watkins, Elizabeth B. White, Yexin Yang

Competing Interests

The authors declare no competing interests

158

159 **Materials and Methods**

160 **Ethics Statement**

161 This study was approved by Yale Human Research Protection Program Institutional Review Boards
162 (FWA00002571, Protocol ID. 2000027690). Informed consents were obtained from all enrolled patients.
163 The healthy blood samples were obtained under the protocol (HIC 0901004619) before the onset of
164 COVID-19 outbreak.

165 **Chemicals**

166 Tributylamine was purchased from Millipore Sigma. LCMS grade water, methanol, isopropanol,
167 chloroform and acetic acid were purchased through Fisher Scientific. All lipid mediator standards were
168 purchased from Cayman Chemical.

169 **Kits and Reagents**

170 CBA kits were purchased from BD Biosciences.

171 **Patient cohort and serum collection**

172 Patients were recruited among those who were admitted to the Yale-New Haven Hospital between
173 March 18th and May 9th, 2020 and were positive for SARS-CoV-2 by RT-PCR from nasopharyngeal
174 and/or oropharyngeal swabs. Patients in this study were enrolled through the IMPACT biorepository
175 study after obtaining informed consent. Basic demographics and clinical information of study
176 participants were obtained and shown in Table 1.
177 Prior to thawing, all samples were gamma-irradiated (2 MRad) to inactivate potential infectious virus.

178 **Sample processing for aqueous, organic, and lipid mediator extraction**

179 For all LCMS methods LCMS grade solvents were used. Sample order was randomized throughout each
180 extraction. For aqueous and organic metabolites, 50 µL patient serum was aliquoted directly into 400 µL
181 of ice-cold methanol and 500 µL of ice-cold chloroform was added. Samples were agitated by shaking for

182 20 minutes at 4 °C and subsequently centrifuged at 16k xg for 20 minutes at 4 °C to induce layering. The
183 top (aqueous) layer and bottom (organic layer) were collected. The aqueous layer was diluted 1:10 in
184 50% methanol in water and prepared for LCMS injection. The organic layer was taken to dryness in a
185 Savant™ DNA120 SpeedVac™ concentrator (Thermo Fisher) and stored at -80 °C until analysis. At time of
186 analysis, samples were resuspended in 500 µL of 5 µg/mL butylated hydroxytoluene in 6:1
187 isopropanol:methanol and further diluted 1:3 in the same solvent combination for LC-M/MS injection.

188 **Lipid mediators sample processing and extraction**

189 Lipid mediators were extracted from patient serum as previously described.[44] Briefly 100 µL of serum
190 was aliquoted on ice and 1 ng each of d8-5-HETE, d5-RvD2, d5-LXA4, d4-LTB4, d4-PGE2 was added to
191 each sample followed by 400 µL of ice-cold methanol. Samples were incubated for 30 min at -20 °C to
192 allow precipitation of protein. Samples were centrifuged at 10k xg for 10 minutes and the supernatant
193 was collected in a fresh tube.

194 Solid phase extraction columns (Sep-Pak® 3 mL, 200 mg, C18, Waters Corporation) were conditioned in
195 vacuum manifold with 10 mL of methanol followed by 10 mL of water. One at a time to each
196 supernatant, 9 mL of acidified water (pH 3.5 with hydrochloric acid) was added and the samples was
197 quickly loaded onto column. The column was then washed to with 10 mL of water. Once samples were
198 loaded, columns were washed with 4 mL of hexanes and then lipid mediators were eluted with 8 mL of
199 methyl-formate. Samples were dried under nitrogen and resuspended in 100 µL of 1:1 water:methanol.
200 For LC-MS analysis 30 µL of each sample was injected.

201 **LC-MS/MS analysis**

202 Aqueous metabolite, lipid, and lipid mediator samples were analyzed using a series of targeted multiple-
203 reaction monitoring (MRM) methods. All samples were separated using a Sciex ExionLC™ AC system and
204 analyzed using a Sciex 5500 QTRAP® mass spectrometer.

205 Aqueous metabolites were analyzed using a previously established ion pairing method with
206 modification.[14] Quality control samples were injected after every 10 injections and assessed for signal
207 stability. Samples were separated across a Waters Atlantis T3 column (100Å, 3 µm, 3 mm X 100 mm) and
208 eluted using a binary gradient from 5 mM tributylamine, 5 mM acetic acid in 2% isopropanol, 5%
209 methanol, 93% water (v/v) to 100% isopropanol over 15 minutes. Analytes were detected in negative
210 mode using two distinct MRM pairs for each metabolite when possible. After signal confirmation only
211 one of the MRM signals was taken forward for analysis. Heavy labeled standards were not utilized given
212 the breadth of targets, thus relative quantification was performed. Fidelity of select signals including
213 retention time and spectra was confirmed by comparison to a synthetic molecular reference.
214 Lipid samples were analyzed using a previously established HILIC method with modification.[13] Samples
215 were separated on a Water XBridge® Amide column (3.5 µm, 3 mm X 100 mm) and eluted using a 12
216 minute binary gradient from 100% 5 mM ammonium acetate, 5% water in acetonitrile apparent pH 8.4
217 to 95% 5 mM ammonium acetate, 50% water in acetonitrile apparent pH 8.0. Target lipids were
218 detected using scheduled MRM. Lipid signals were divided into two methods utilizing either negative
219 mode or positive mode and a separate injection was analyzed for each method. Both datasets were
220 separately normalized using total-area sum to correct for instrument drift.
221 Lipid mediators were analyzed using a previously established reverse phase method with
222 modifications.[44] Samples were separated on a Waters Atlantis T3 column (100Å, 3 µm, 3 mm X 100 mm)
223 and using a binary gradient of A: 0.01 % acetic acid in water and B: 0.01 % acetic acid in methanol.
224 Samples were eluted over 20 min from 40-100 % B. Samples were detected in negative mode using
225 previously published MRM pairs and source conditions.[36] Triggered spectra were collected using
226 enhanced-product ion scans and rolling collision energy. A blank and a standard mix were serially
227 injected every 10 injections. Standard mix consisted of each of the following compounds at 10 ng/mL:
228 RvE3, LXA4, LXA5, LXB4, PGE2, PGD2, PGF2a, TxB2, PD1, RvD5, Maresin 1, LTB4, 5,15-DiHETE, 14-HDHA,

229 18-HEPE, AA, EPA, DHA. Spectra and comparison to authentic standards was used to confirm signal
230 identity.
231 Spectral confirmation was not possible for RvD2, RvD3, LXA5, RvD6, 8,9 DiHETrE, 12-HHT, 11-HETE, 11-
232 HEPE, 7-HDPA, 13-HDPA, 14-HDPA, 17-HDPA, 7-HDHA, 13-HDHA, 17-HDHA and 21-HDHA but identity
233 was assessed by comparison to related standards. These signals were regarded as lower confidence but
234 were used for class comparison of the LMs and multivariate analysis.
235 All signals were integrated using MultiQuant® Software 3.0.3. In total 1,414 molecules were targeted
236 across a water-soluble metabolite method and two organic-extracted lipid methods in either positive or
237 negative ionization modes. Of these 716 features were judged to be positively detected by visual
238 inspection, missing value filtering (50% cut-off) and QC coefficient of variance filtering (40% cut-off after
239 normalization). Remaining missing values were replaced with the minimum group value for that feature.
240 For aqueous and lipid mediator datasets signal quality was judged visually and signal stability was
241 assessed by QC or repeat injection of a standard mix. Lipid mediator data was normalized to internal
242 heavy isotope standards as previously described.[44]
243 Univariate and multivariate analysis was performed in MarkerView® Software 1.3.1. The aqueous
244 dataset and the combined lipid mediators/cytokine dataset data were autoscaled prior to multivariate
245 analysis in order to visualize the contribution of low ionization efficiency species and difference of scales
246 between the cytokine and lipid mediator measurements. Lipid datasets were pareto scaled to avoid
247 overrepresenting low abundance signals within each lipid class. For all univariate analysis an unpaired t-
248 test was used. For univariate analysis of the LM/cytokine set a single moderate group patient was
249 excluded by an extreme studentized deviate test for analysis of PGE2 ($z = 4.58$).
250 **Quantification of cytokine and chemokine levels**
251 The serum concentration of IFN-α, IFN-γ, IL-1β, IL-2, IL-4, IL-6, IL-8, IL-10, IL-12/IL-23p40, IL-17A, MIP-1α,
252 RANTES, TNF-α, and MCP-1 was determined using a cytometric bead array according to the

253 manufacturer's instructions (BD Biosciences). The serum concentration of IL-1α was determined by an
254 ELISA according to the manufacturer's instructions (R & D Systems).

255 **Single cell RNA sequencing analysis**

256 The published single cell RNA sequencing dataset from Wilk, et al Nature Medicine 2020 was
257 downloaded from the COVID-19 Cell Atlas (https://www.covid19cellatlas.org/#wilk20).[38] Data was read
258 into Seurat v3.0 and each cluster's cellular identity was annotated per Wilk, et al Nature Medicine
259 2020.[38] Expression levels of ALOX and CYP genes within specific cell types in healthy controls and COVID-
260 19 patients was visualized using Seurat's DotPlot feature. *ALOX5* expression levels in specific cell types
261 was visualized using the VlnPlot feature A Mann-Whitney test was used to determine statistical
262 differences in gene expression between healthy and COVID samples.

263 **Patient Statistics**

264 Demographic data is presented as either counts and percentages (for categorical data) or means and
265 standard deviations (for continuous data). To investigate the difference in the control, moderate and
266 severe groups, GraphPad Prism (version 8.4.2) was used. The results were compared using the chi-
267 square test or Fisher's exact test for categorical variables and one-way analysis of variance (ANOVA) or
268 unpaired t test was used for continuous variables. A p-value of less than 0.05 was considered statistically
269 significant.

270

271 **References**

272 1. Richardson, S.*, et al.* Presenting characteristics, comorbidities, and outcomes among 5700
273 patients hospitalized with COVID-19 in the New York City area. *Jama* (2020).

274 2. Braverman, N.E. & Moser, A.B. Functions of plasmalogen lipids in health and disease. *Biochimica*
275 *et Biophysica Acta (BBA)-Molecular Basis of Disease* **1822**, 1442-1452 (2012).

276 3. Yang, J.*, et al.* Prevalence of comorbidities in the novel Wuhan coronavirus (COVID-19) infection:
277 a systematic review and meta-analysis. *International journal of infectious diseases* (2020).

278 4. Bellis, C.*, et al.* Human plasma lipidome is pleiotropically associated with cardiovascular risk
279 factors and death. *Circulation: Cardiovascular Genetics* **7**, 854-863 (2014).

280 5. Pietiläinen, K.H.*, et al.* Association of lipidome remodeling in the adipocyte membrane with
281 acquired obesity in humans. *PLoS Biol* **9**, e1000623 (2011).

282 6. Sharma, S.*, et al.* Role of oxidized lipids in pulmonary arterial hypertension. *Pulmonary*
283 *circulation* **6**, 261-273 (2016).

284 7. Titz, B.*, et al.* Alterations in serum polyunsaturated fatty acids and eicosanoids in patients with
285 mild to moderate chronic obstructive pulmonary disease (COPD). *International journal of*
286 *molecular sciences* **17**, 1583 (2016).

287 8. Pettersen, D., Davidsson, Ö. & Whatling, C. Recent advances for FLAP inhibitors. *Bioorganic &*
288 *Medicinal Chemistry Letters* **25**, 2607-2612 (2015).

289 9. Blasco, H.*, et al.* The specific metabolome profiling of patients infected by SARS-COV-2 supports
290 the key role of tryptophan-nicotinamide pathway and cytosine metabolism. (Research Square,
291 2020).

292 10. Shen, B.*, et al.* Proteomic and metabolomic characterization of COVID-19 patient sera. *Cell*
293 (2020).

294 11. Troisi, J.*, et al.* Serum metabolomic profile of symptomatic and asymptomatic SARS-CoV-2
295 infected patients. (2020).
296 12. Wu, D.*, et al.* Plasma Metabolomic and Lipidomic Alterations Associated with COVID-19.
297 *medRxiv* (2020).
298 13. Mackenzie Pearson, S.K.K., Wu, S. & Baker, P.R. Achieve Broad Lipid Quantitation using a High-
299 Throughput Targeted Lipidomics Method.
300 14. McCloskey, D., Gangoiti, J.A., Palsson, B.O. & Feist, A.M. A pH and solvent optimized reverse-
301 phase ion-paring-LC–MS/MS method that leverages multiple scan-types for targeted absolute
302 quantification of intracellular metabolites. *Metabolomics* **11**, 1338-1350 (2015).
303 15. Dawson, J. & Walters, M. Uric acid and xanthine oxidase: future therapeutic targets in the
304 prevention of cardiovascular disease? *British journal of clinical pharmacology* **62**, 633-644
305 (2006).
306 16. Hare, J.M. & Johnson, R.J. Uric acid predicts clinical outcomes in heart failure: insights regarding
307 the role of xanthine oxidase and uric acid in disease pathophysiology. (Am Heart Assoc, 2003).
308 17. Papi, A.*, et al.* Role of xanthine oxidase activation and reduced glutathione depletion in
309 rhinovirus induction of inflammation in respiratory epithelial cells. *Journal of Biological*
310 *Chemistry* **283**, 28595-28606 (2008).
311 18. Tobin, M.J., Laghi, F. & Jubran, A. Why COVID-19 Silent Hypoxemia is Baffling to Physicians.
312 *American Journal of Respiratory and Critical Care Medicine* (2020).
313 19. Chen, X.-Q., Dong, J., Niu, C.-Y., Fan, J.-M. & Du, J.-Z. Effects of hypoxia on glucose, insulin,
314 glucagon, and modulation by corticotropin-releasing factor receptor type 1 in the rat.
315 *Endocrinology* **148**, 3271-3278 (2007).
316 20. Newhouse, L.P.*, et al.* Three hours of intermittent hypoxia increases circulating glucose levels in
317 healthy adults. *Physiological reports* **5**, e13106 (2017).

318 21. Oltmanns, K.M.*, et al.* Hypoxia causes glucose intolerance in humans. *American journal of*
319 *respiratory and critical care medicine* **169**, 1231-1237 (2004).
320 22. Xie, J.*, et al.* Association between hypoxemia and mortality in patients with COVID-19. in *Mayo*
321 *Clinic Proceedings* (Elsevier, 2020).
322 23. Reis, A.*, et al.* A comparison of five lipid extraction solvent systems for lipidomic studies of
323 human LDL. *Journal of lipid research* **54**, 1812-1824 (2013).
324 24. Tyagi, R.K., Azrad, A., Degani, H. & Salomon, Y. Simultaneous extraction of cellular lipids and
325 water-soluble metabolites: evaluation by NMR spectroscopy. *Magnetic resonance in medicine*
326 **35**, 194-200 (1996).
327 25. Lin, C.Y., Wu, H., Tjeerdema, R.S. & Viant, M.R. Evaluation of metabolite extraction strategies
328 from tissue samples using NMR metabolomics. *Metabolomics* **3**, 55-67 (2007).
329 26. Lebrero, P.*, et al.* Cellular plasmalogen content does not influence arachidonic acid levels or
330 distribution in macrophages: A role for cytosolic phospholipase A2γ in phospholipid remodeling.
331 *Cells* **8**, 799 (2019).
332 27. Dennis, E.A. & Norris, P.C. Eicosanoid storm in infection and inflammation. *Nature Reviews*
333 *Immunology* **15**, 511-523 (2015).
334 28. Norris, P.C., Gosselin, D., Reichart, D., Glass, C.K. & Dennis, E.A. Phospholipase A2 regulates
335 eicosanoid class switching during inflammasome activation. *Proceedings of the National*
336 *Academy of Sciences* **111**, 12746-12751 (2014).
337 29. Dennis, E.A., Cao, J., Hsu, Y.-H., Magrioti, V. & Kokotos, G. Phospholipase A2 enzymes: physical
338 structure, biological function, disease implication, chemical inhibition, and therapeutic
339 intervention. *Chemical reviews* **111**, 6130-6185 (2011).
340 30. Lämmermann, T.*, et al.* Neutrophil swarms require LTB4 and integrins at sites of cell death in
341 vivo. *Nature* **498**, 371-375 (2013).

342 31. Bitto, A.*, et al.* Flavocoxid, a dual inhibitor of COX-2 and 5-LOX of natural origin, attenuates the
343 inflammatory response and protects mice from sepsis. *Critical Care* **16**, R32 (2012).
344 32. Dalli, J. & Serhan, C.N. Specific lipid mediator signatures of human phagocytes: microparticles
345 stimulate macrophage efferocytosis and pro-resolving mediators. *Blood* **120**, e60-e72 (2012).
346 33. Kowal-Bielecka, O.*, et al.* Cyclooxygenase-and lipoxygenase-derived eicosanoids in
347 bronchoalveolar lavage fluid from patients with scleroderma lung disease: An imbalance
348 between proinflammatory and antiinflammatory lipid mediators. *Arthritis & Rheumatism* **52**,
349 3783-3791 (2005).
350 34. Serhan, C.N. & Haeggstrom, J. Lipid mediators in acute inflammation and resolution:
351 Eicosanoids, PAF, resolvins, and protectins. *Fundamentals of Inflammation. CN Serhan, PA Ward,*
352 *DW Gilroy, and SS Ayoub, editors. Cambridge University Press, Cambridge*, 153-174 (2010).
353 35. Serhan, C.N. & Savill, J. Resolution of inflammation: the beginning programs the end. *Nature*
354 *immunology* **6**, 1191-1197 (2005).
355 36. Ian Riley, P.C.N., Kathy Luong, Charles Serhan. CET&RI Spectra Book & Physical Properties of
356 SPM and Eicosanoids 2019. (2019).
357 37. Tam, V.C.*, et al.* Lipidomic profiling of influenza infection identifies mediators that induce and
358 resolve inflammation. *Cell* **154**, 213-227 (2013).
359 38. Wilk, A.J.*, et al.* A single-cell atlas of the peripheral immune response in patients with severe
360 COVID-19. *Nature Medicine*, 1-7 (2020).
361 39. Liao, M.*, et al.* Single-cell landscape of bronchoalveolar immune cells in patients with COVID-19.
362 *Nature medicine*, 1-3 (2020).
363 40. Merad, M. & Martin, J.C. Pathological inflammation in patients with COVID-19: a key role for
364 monocytes and macrophages. *Nature Reviews Immunology*, 1-8 (2020).

365 41. Renaud, H.J., Cui, J.Y., Khan, M. & Klaassen, C.D. Tissue distribution and gender-divergent
366 expression of 78 cytochrome P450 mRNAs in mice. *Toxicological sciences* **124**, 261-277 (2011).
367 42. Huang, C.*, et al.* Clinical features of patients infected with 2019 novel coronavirus in Wuhan,
368 China. *The lancet* **395**, 497-506 (2020).
369 43. Kalinski, P. Regulation of immune responses by prostaglandin E2. *The Journal of Immunology*
370 **188**, 21-28 (2012).
371 44. English, J.T., Norris, P.C., Hodges, R.R., Dartt, D.A. & Serhan, C.N. Identification and profiling of
372 specialized pro-resolving mediators in human tears by lipid mediator metabolomics.
373 *Prostaglandins, Leukotrienes and Essential Fatty Acids* **117**, 17-27 (2017).

374

375

376 **Figure Captions**

377 **Figure 1. Mobilization of plasmalogen-derived PUFAs correlates with the disease severity in COVID-19.**
378 **(a)** Supervised PLSDA analysis of the healthy, moderate and severe disease groups and **(b)** the
379 corresponding feature loading plot. (c-e) Comparison of moderate to healthy **(c)**, severe to healthy **(d)**
380 and severe to moderate **(e)** by unpaired t-test with PUFA classes overlaid. Overlaid data series
381 correspond to lipid species containing at least one copy of C20:4 (blue), C20:5 (orange), C22:5 (purple)
382 or C22:6 (red) acyl chains. **(f-h)** Comparison of moderate to healthy **(f)**, severe to healthy **(g)** and severe
383 to moderate **(h)** by unpaired t-test with plasmalogen lipid series overlaid in red. For (c-h) cutoff lines
384 indicate a positive or negative 2-fold change and a p-value of 0.05. **(i-l)** Heatmap of the autoscaled mean
385 intensity of each patient group for significantly varied lipids ($p<0.05$) containing C20:4 **(i)**, C20:5 **(j)**, C22:5
386 **(k)**, and C22:6 **(l)**. Color scale is consistent for (i-l).

387

388 **Figure 2: A unique milieu of LMs defines moderate and severe COVID-19 disease. (a)** Unsupervised PCA
389 of autoscaled combined lipid mediator and cytokine dataset and **(b)** corresponding feature loading plot.
390 **(c-e)** Univariate comparison of moderate disease to healthy **(c)**, severe disease to healthy **(d)** and severe
391 to moderate disease **(f)** by unpaired t-test. Cutoff lines indicate a positive or negative 2-fold change and
392 a p-value of 0.05. For (b-f) species are colored by class as cytokine (cyan), arachidonic acid-derived (AA-
393 derived, blue), eicosapentaenoic acid-derived (EPA-derived, orange), docosapentaenoic acid-derived
394 (DPA-derived, purple) or docosahexaenoic acid-derived (DHA-derived, red). **(f-k)** Heatmaps of the
395 autoscaled mean for each patient group across cytokines **(f)**, molecules synthesized by ALOX5 **(g)**,
396 ALOX12 **(h)**, ALOX15 **(i)**, Cyclooxygenases **(j)** or cytochrome P450 **(k)**. Color scale is consistent across (f-
397 k).

398

399 **Figure 3. Human PBMCs from COVID-19 patients are enriched for *ALOX5* expressing cells and express**

400 **higher levels of *ALOX5*. (a)** UMAP dimensionality reduction plot of a published human PBMC single-cell

401 RNA Seq dataset (Wilk, et al *Nature Medicine* 2020) identifying twenty cell types. **(b)** UMAP depicting

402 *ALOX5* expressing cells in blue. **(c)** Violin plots indicating *ALOX5* expression levels within specific cellular

403 populations in healthy (blue) or COVID (red) PBMCs. Statistical significance was determined by a Mann-

404 Whitney test; * $p < 0.05$. ** $p < 0.01$.

405

406

407 **Table 1. Patient demographics, preexisting conditions and treatment distributions.** Patient data were

408 compared using the chi-square test or Fisher's exact test for categorical variables and one-way analysis

409 of variance (ANOVA) or unpaired t test was used for continuous variables.

	Healthy (n=19)	Moderate (n=18)	Severe (n=20)	p-value
Demographics				
Mean Age ± SD (Range)	42.7 ± 14.92 (21-72）	60.56 ± 14.11 (26-92)	63.6 ± 15.17 (32-91）	<0.001
Mean BMI ± SD (Range)		29.65 ± 8.37 (19.49-55.04)	31.08 ± 5.84 (22.87-44)	0.5402
Gender, n (%)				0.6391
Male	9 (47.37%)	11 (61.11%)	12 (60%)	
Female	10 (52.63%)	7 (38.89%)	8 (40%)	
Race, n (%)				0.8932
White	15 (78.95%）	13 (72.22%)	14 (70%)	
Black	2 (10.53%）	2 (11.11%)	3 (15%)	
Hispanic	1 (5.26%）	2 (11.11%)	3 (15%)	
Asian	1 (5.26%）	1 (5.56%)	0 (0%)	
Comorbidities				
Heart disease		5 (27.78%)	10 (50%)	0.1983
Hyperlipidemia		4 (22.22%)	6 (30%)	0.719
Hypertension		10 (55.56%)	15 (75%)	0.3071
Chronic lung diseases		1 (5.56%)	4 (20%)	0.3436
Diabetes		5 (27.78%)	7 (35%)	0.7342
Therapies				
Tociluzimab		9 (50%)	18 (90%)	0.0113
Hydroxycloroquine		13 (72.22%)	20 (100%)	0.0171
Steroids		2 (11.11%)	8 (40%)	0.0673
Antiviral				0.5292
Azatanavir		11 (61.11%)	13 (65%)	
Remdesivir trial		2 (11.11%)	4 (20%)	
Mechanical ventilation		0 (0%)	13 (65%)	<0.0001
Intensive Care Unit		0 (0%)	20 (100%)	<0.0001

410

Figure 1

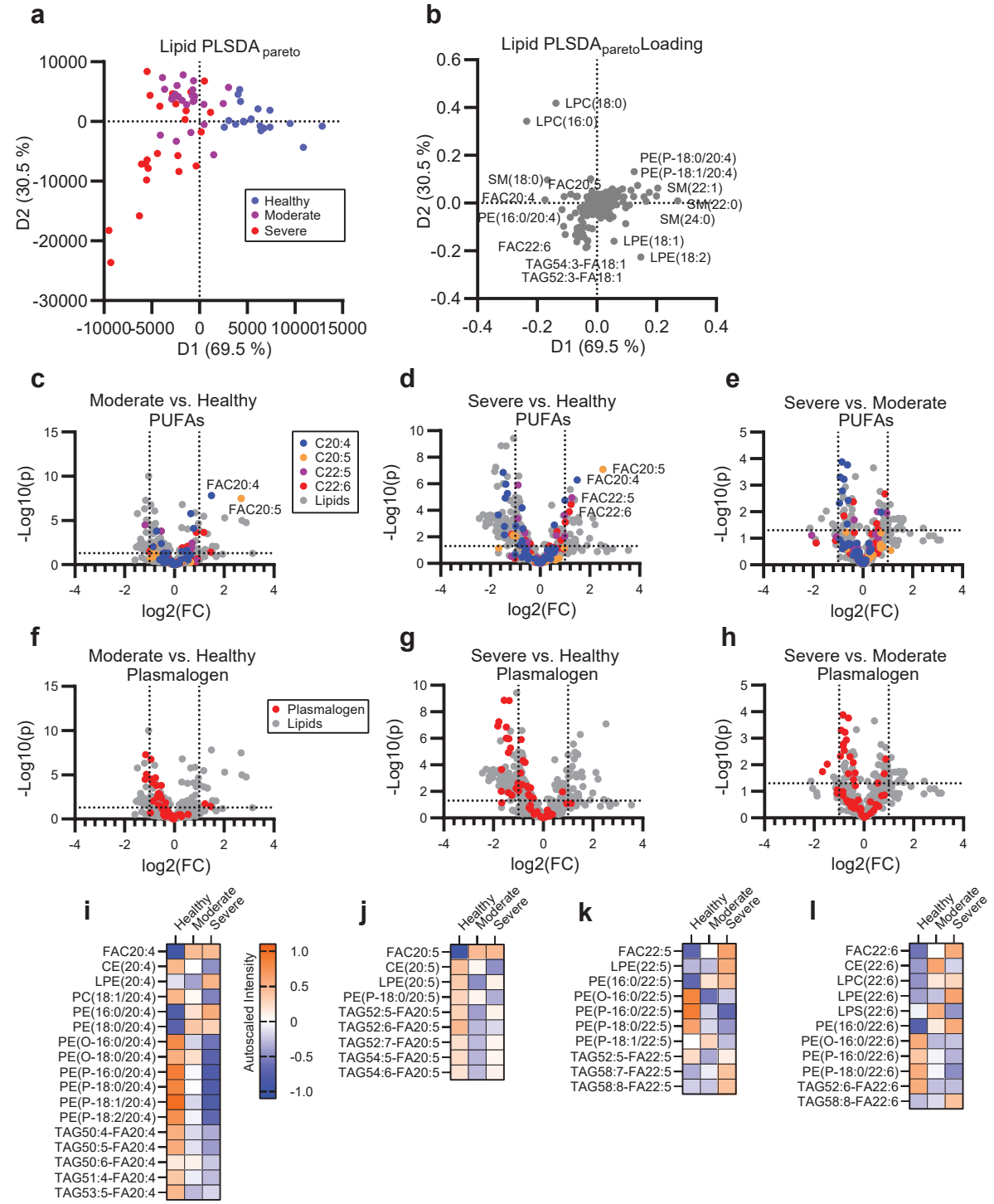
a
Lipid PLSDA pareto
D2 (30.5 %)
D1 (69.5 %)
Healthy
Moderate
Severe
b
Lipid PLSDA pareto Loading
LPC(18:0)
LPC(16:0)
PE(P-18:0/20:4)
PE(P-18:1/20:4)
SM(22:1)
SM(22:0)
SM(24:0)
LPE(18:1)
LPE(18:2)
SM(18:0)
FAC20:5
FAC20:4
PE(16:0/20:4)
FAC22:6
TAG54:3-FA18:1
TAG52:3-FA18:1
c
Moderate vs. Healthy PUFAs
FAC20:4
FAC20:5
C20:4
C20:5
C22:5
C22:6
Lipids
-Log10(p)
log2(FC)
d
Severe vs. Healthy PUFAs
FAC20:5
FAC20:4
FAC22:5
FAC22:6
e
Severe vs. Moderate PUFAs
f
Moderate vs. Healthy Plasmalogen
Plasmalogen
Lipids
g
Severe vs. Healthy Plasmalogen
h
Severe vs. Moderate Plasmalogen
i
Healthy
Moderate
Severe
FAC20:4
CE(20:4)
LPE(20:4)
PC(18:1/20:4)
PE(16:0/20:4)
PE(18:0/20:4)
PE(O-16:0/20:4)
PE(O-18:0/20:4)
PE(P-16:0/20:4)
PE(P-18:0/20:4)
PE(P-18:1/20:4)
PE(P-18:2/20:4)
TAG50:4-FA20:4
TAG50:5-FA20:4
TAG50:6-FA20:4
TAG51:4-FA20:4
TAG53:5-FA20:4
Autoscaled Intensity
1.0
0.5
0
-0.5
-1.0
j
FAC20:5
CE(20:5)
LPE(20:5)
PE(P-18:0/20:5)
TAG52:5-FA20:5
TAG52:6-FA20:5
TAG52:7-FA20:5
TAG54:5-FA20:5
TAG54:6-FA20:5
k
FAC22:5
LPE(22:5)
PE(16:0/22:5)
PE(O-16:0/22:5)
PE(P-16:0/22:5)
PE(P-18:0/22:5)
PE(P-18:1/22:5)
TAG52:5-FA22:5
TAG58:7-FA22:5
TAG58:8-FA22:5
l
FAC22:6
CE(22:6)
LPC(22:6)
LPE(22:6)
LPS(22:6)
PE(16:0/22:6)
PE(O-16:0/22:6)
PE(P-16:0/22:6)
PE(P-18:0/22:6)
TAG52:6-FA22:6
TAG58:8-FA22:6

Figure 2

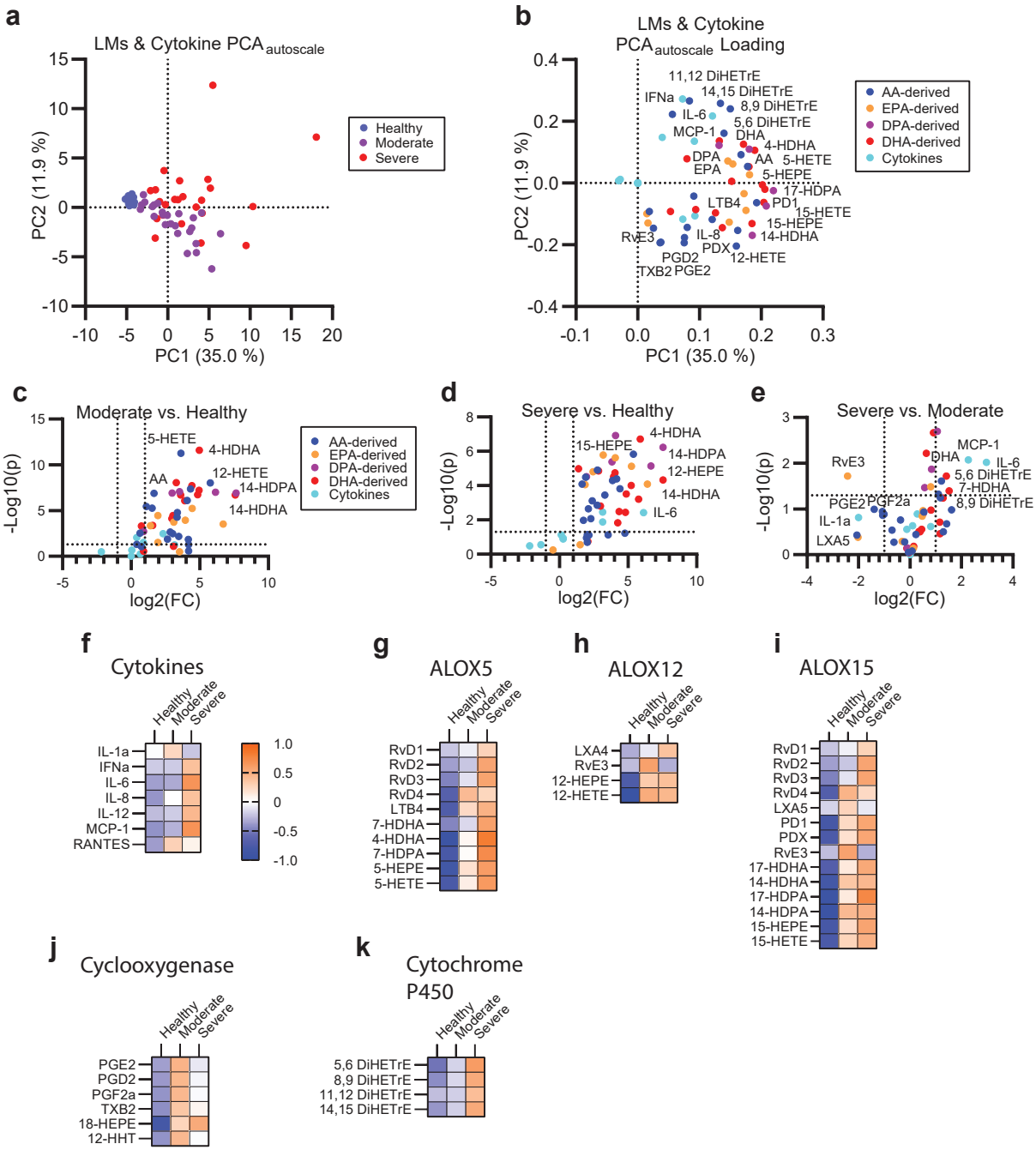
a
LMs & Cytokine PCA autoscale
PC2 (11.9 %)
PC1 (35.0 %)
Healthy
Moderate
Severe
b
LMs & Cytokine PCA autoscale Loading
11,12 DiHETrE
14,15 DiHETrE
8,9 DiHETrE
5,6 DiHETrE
IFNa
IL-6
MCP-1
DHA
4-HDHA
AA
5-HETE
DPA
EPA
5-HEPE
17-HDPA
LTB4
PD1
15-HETE
15-HEPE
RvE3
IL-8
14-HDHA
PDX
12-HETE
PGD2
TXB2
PGE2
AA-derived
EPA-derived
DPA-derived
DHA-derived
Cytokines
c
Moderate vs. Healthy
-Log10(p)
log2(FC)
5-HETE
4-HDHA
AA
12-HETE
14-HDPA
14-HDHA
d
Severe vs. Healthy
15-HEPE
4-HDHA
14-HDPA
12-HEPE
14-HDHA
IL-6
e
Severe vs. Moderate
MCP-1
DHA
IL-6
RvE3
5,6 DiHETrE
7-HDHA
8,9 DiHETrE
PGE2
PGF2a
IL-1a
LXA5
f
Cytokines
Healthy
Moderate
Severe
IL-1a
IFNa
IL-6
IL-8
IL-12
MCP-1
RANTES
1.0
0.5
0
-0.5
-1.0
g
ALOX5
RvD1
RvD2
RvD3
RvD4
LTB4
7-HDHA
4-HDHA
7-HDPA
5-HEPE
5-HETE
h
ALOX12
LXA4
RvE3
12-HEPE
12-HETE
i
ALOX15
RvD1
RvD2
RvD3
RvD4
LXA5
PD1
PDX
RvE3
17-HDHA
14-HDHA
17-HDPA
14-HDPA
15-HEPE
15-HETE
j
Cyclooxygenase
PGE2
PGD2
PGF2a
TXB2
18-HEPE
12-HHT
k
Cytochrome P450
5,6 DiHETrE
8,9 DiHETrE
11,12 DiHETrE
14,15 DiHETrE

Figure 3

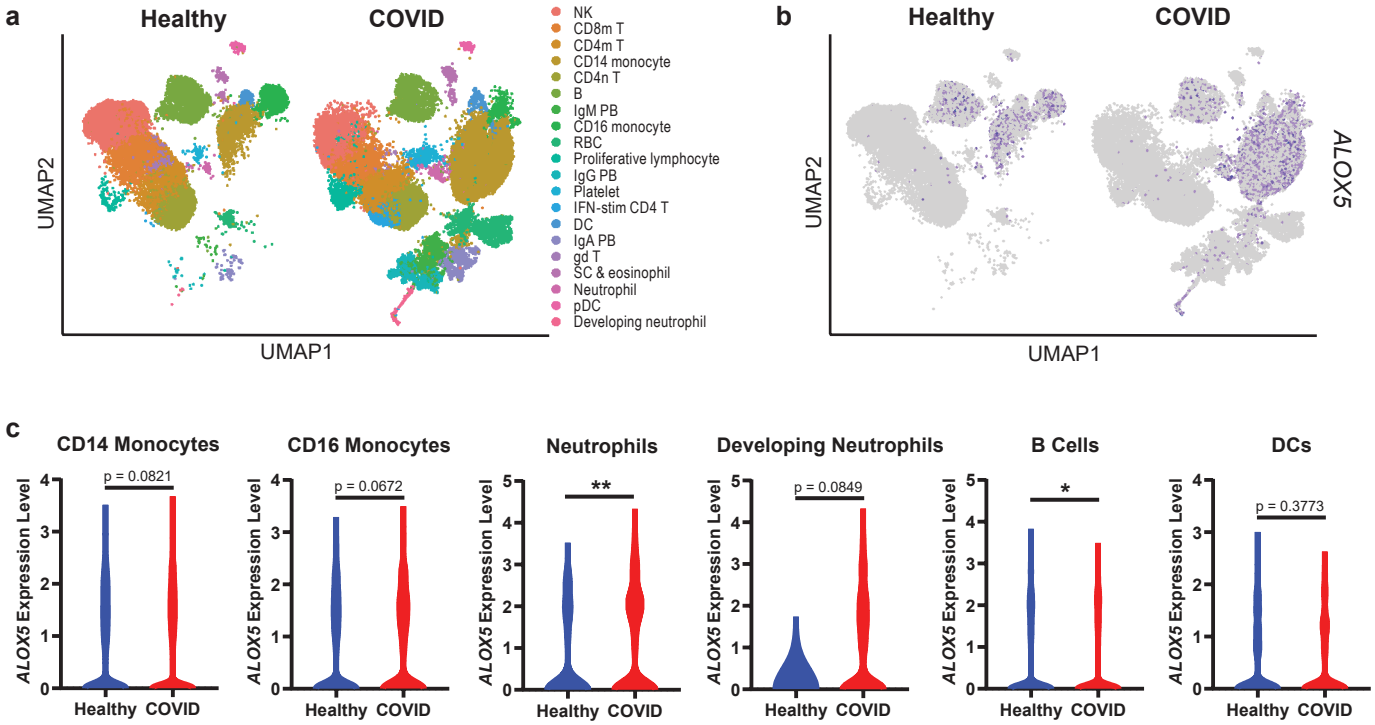
a
Healthy
COVID
UMAP2
UMAP1
NK
CD8m T
CD4m T
CD14 monocyte
CD4n T
B
IgM PB
CD16 monocyte
RBC
Proliferative lymphocyte
IgG PB
Platelet
IFN-stim CD4 T
DC
IgA PB
gd T
SC & eosinophil
Neutrophil
pDC
Developing neutrophil
b
Healthy
COVID
UMAP2
UMAP1
ALOX5
c
CD14 Monocytes
CD16 Monocytes
Neutrophils
Developing Neutrophils
B Cells
DCs
ALOX5 Expression Level
p = 0.0821
p = 0.0672
**
p = 0.0849
*
p = 0.3773
Healthy
COVID